

Tyler Anderson
Evgeniya Akatyeva
Ilia Nikiforov

Department of Mechanical Engineering,
University of Minnesota,
Minneapolis, MN 55455

David Potyondy
Itasca Consulting Group, Inc.,
111 Third Avenue South,
Minneapolis, MN 55401

Roberto Ballarini
Department of Civil Engineering,
University of Minnesota,
Minneapolis, MN 55455

Traian Dumitrică¹
Department of Mechanical Engineering,
University of Minnesota,
Minneapolis, MN 55455
e-mail: td@me.umn.edu

Toward Distinct Element Method Simulations of Carbon Nanotube Systems

We propose distinct element method modeling of carbon nanotube systems. The atomic-level description of an individual nanotube is coarse-grained into a chain of spherical elements that interact by parallel bonds located at their contacts. The spherical elements can lump multiple translational unit cells of the carbon nanotube and have both translational and rotational degrees of freedom. The discrete long ranged interaction between nanotubes is included in a van der Waals contact of nonmechanical nature that acts simultaneously with the parallel bonds. The created mesoscopic model is put into service by simulating a realistic carbon nanotube ring. The ring morphology arises from the energy balance stored in both parallel and van der Waals bonds.

[DOI: 10.1115/1.4002609]

1 Introduction

Carbon nanotubes (CNTs) exhibit remarkable mechanical characteristics such as high mechanical strength [1] and resilience [2]. For this reason, they are highly researched for applications. Valuable insights into individual CNT response have been obtained theoretically from atomic-level simulations [1–5]. Unfortunately, performing exhaustive simulations at atomistic scale for CNT systems of engineering significance is computationally prohibitive. Coarse-graining approaches that reduce [6,7], combine [8], or even eliminate [9,10] the large number of atomistic degrees of freedom are used in order to make simulations manageable. However, in spite of such developments, simulations on collective behavior have not kept pace with the demand from many areas ranging from nanoelectromechanical systems [11], nanocomposite materials [12], and nanotoxicology [13].

To model large-scale motions of polymers, colloids, surfactants, nanotubes, and biomolecular assemblies, mesoscopic simulation methods have been developed such as dissipative particle dynamics [14] and Langevin dynamics [15]. Interestingly, the method invoked here, the distinct element method (DEM) [16], is currently used for larger scale simulations in granular and discontinuous materials such as granular flows, powder mechanics, and rock mechanics [17]. In this work, we show that DEM can be easily adapted for CNT simulations. We first formulate a basic DEM mesoscopic model of CNT systems in terms of the contact interactions between discrete elements. Using parameters derived previously from the atomic-level description, we illustrate the utility of this model in a complex situation involving large elastic deformation and van der Waals (vdW) adhesion. DEM emerges as an attractive methodology not only because of its simplicity but also because of its availability in several commercially available distinct element programs such as PFC3D [18] (which was used to perform the work described here). It may also be possible to per-

form similar modeling with traditional molecular dynamics programs such as LAMMPS [19].

2 Distinct Element Method for CNTs

Unlike other particle-based methods, the DEM particles are no longer being treated as point masses. Instead, each individual element is a rigid body characterized by a mass m uniformly distributed in the spherical element of radius R and moment of inertia $I=(2/5)mR^2$. These parameters are time-independent, and for simplicity, here all spheres are taken to be identical. Thus, the system composed of a collection of N discrete element contains not only translational but also rotational degrees of freedom. Specifically, the generalized coordinates (also called state variables) are the positions \mathbf{r}_i and velocities \mathbf{v}_i for the center of mass of each sphere, as well as their angular rotations Θ_i and angular velocity vectors Ω_i , where $i=1, \dots, N$.

One counterintuitive aspect is that although the spherical particles are rigid, they can interpenetrate, Fig. 1. The intersection of the two proximate spherical surfaces define a plane, the contact plane, perpendicular to the axis connecting the two centers located at \mathbf{r}_i and \mathbf{r}_{i+1} . In the DEM logic, interpenetration signifies that the two elements interact. Various constitutive contact models of pure mechanical nature are available [18] to describe the interaction of elements. The mechanical behavior of this system is described by evolving in time each rigid sphere according to the laws of classical mechanics $\mathbf{F}_i=m\ddot{\mathbf{r}}_i$ and $\mathbf{M}_i=I\ddot{\Theta}_i$. \mathbf{F}_i and \mathbf{M}_i are the total force and moment, respectively, acting on element i that arise due to the interactions with the elements in contact, as well as artificially introduced dissipative forces. With the PFC3D method at hand [18], the system is evolved in time with a nonsymplectic leapfrog second-order in time-step scheme. The goal is to drive the system toward a low energy metastable state rather than performing thermodynamic integration like in molecular dynamics.

2.1 Contact Model to Represent the Covalent Binding. The individual CNT quasi-one-dimensional structure extending over microns of length originates in the strong covalent carbon-carbon

¹Corresponding author.

Manuscript received September 7, 2010; final manuscript received September 14, 2010; published online October 27, 2010. Assoc. Editor: Vijay K. Varadan.

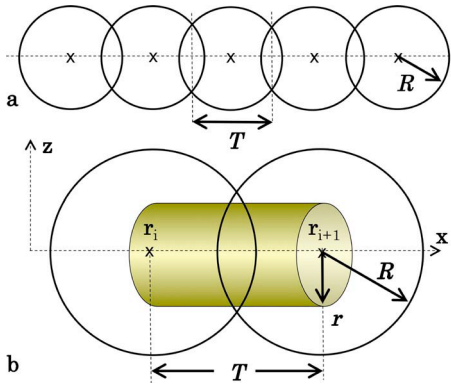


Fig. 1 (a) CNT representation as a chain of overlapping spherical elements shown here in 2D. (b) Parallel bond contact model for the interaction of two spherical elements with radius R .

bonding. This bonding is formed by sharing of the valence electrons according to the laws of quantum mechanics. Paramount to our coarse-grained DEM model is describing the larger scale mechanics. Thus, we aim to retain from the fundamental atomic-scale both quasi-one-dimensional stable structure and low-frequency acoustic vibrations.

As reviewed on a number of occasions [20], the nanomechanics of deformed CNTs can be interpreted with the heuristics of the continuum. For example, a quadratic variation of strain energy with the applied strain computed microscopically is usually interpreted as linear elastic behavior. Recent microscopic data indicated that single-walled CNTs of moderate diameters can be well represented as isotropic elastic continuum shells, as earlier proposed [2]. Under large tensile stress, CNTs fail irreversibly through plasticity or brittle fracture [1]. However, microscopic calculations indicated that CNT also exhibit a rich nonlinearly elastic behavior over wide ranges of mechanical stress [2,4,5]. With the DEM approximation, the continuum behavior can be well reproduced. Thus, the known atomic-scale nanomechanical behavior suggests that the existing DEM clumping structure valid for the macroscale can be used and there is no need to invent a new contact model for this purpose.

The high degree of crystalline uniformity of CNTs naturally associates one spherical element with one translational cell or supercell repeating unit with length T and containing N_a atoms. Thus, in the stress-free representation of a CNT, the distance between contact planes is T (Fig. 1(a)). It is important to recognize that to comply with the underlying atomic-scale description, the translational fragments lumped into the discrete elements cannot be kept frozen during the relative motion of proximate elements with respect to each other. From the existing contact models, we found adequate the standard parallel bond contact because it establishes an elastic interaction between particles in terms of both forces and moments. (The nomenclature used highlights that this contact can work in parallel with other contact models.)

A parallel bond can be envisioned as a finite-sized disk of elastic massless material with radius r bound around the contact and centered on the axis connecting the centers of two proximate elements (Fig. 1(b)). To this disk, we associate a set of ideal elastic springs with normal k_n and shear k_s stiffnesses uniformly distributed over its circular cross section. When the contact is formed in DEM, the total contact force and moment are initialized to zero. A mechanical deformation will reflect in displacements of the generalized coordinates with respect with their initial position and contact elastic forces and moments acting to restore the needlelike shape. The restoring force and a moment develop within the bond material according to its constitutive law. For example, a δx axial relative displacement between i and $i+1$ elements causes a contact restoring force $F_i^x = -F_{i+1}^x = -k_n S \delta x$, while a $\delta \theta^z$ relative angular

displacement causes a contact restoring moment $M_i^x = -M_{i+1}^x = -k_s I_x \delta \theta^z$. Here, $S = \pi r^2$ and $I_x = (\pi/2) r^4$ are the area and the polar moment of inertia of the disk cross section. The full description of the parallel bond implementation in PFC3D can be found in Potyondy and Cundall [17].

The two spring constants can be obtained by considering elastic elongation and torsion deformations and equating the strain energy of the DEM model with the one obtained microscopically. It follows that the length of the parallel bond disk is T and $k_n = Y/T$ and $k_s = G/T$. Here, Y and G are atomistically computed Young and shear moduli, respectively.

2.2 Contact Model to Represent the vdW Interactions. To be able to simulate CNT systems, the parallel bonds representing the covalent binding must be supplemented with a new contact force representing the vdW interaction between two underlying parallel nanotube segments of length T . Fortunately, this interaction can be captured in a simple analytical form. Usually, the vdW interaction between two atoms located at distance d is represented by a Lennard-Jones (LJ) 6-12 potential $v(d) = 4\epsilon[(\sigma/d)^{12} - (\sigma/d)^6]$, where ϵ and σ are standard parameters.² We treat the discrete interaction between carbon atoms located on the two parallel tube segments of length T in continuum way in terms of area density of atoms $\rho_c = 4/(3\sqrt{3}a_{C-C}^2)$ [21]. Here, $a_{C-C} = 1.42$ Å is the equilibrium carbon-carbon bond length in graphene. Integrating the LJ interaction over the surfaces of the two tube segments located at a center-to-center distance L , we arrived at (see Appendix)

$$V(D) \approx 4\epsilon' \left[\frac{A}{D^{9.5}} - \frac{B}{D^{3.5}} \right] \quad (1)$$

Here, $D = (L/r) - 2$ is the normalized intertube center-to-center distance and $\epsilon' = ((3\pi\sigma^6/8r^3)\rho_c^2 T)\epsilon$. $A = (21\sigma^6/32r^6)a$ and values of dimensionless constants a and B are given in the Appendix. This simple form for the vdW interaction energy V makes it easy to derive the vdW force component acting on the spherical elements. While this model assumes that each DEM ball only interacts with its nearest neighbor in the adjacent nanotube segment, it may be easily adapted to the case of multiple-neighbor interactions such as when the DEM balls are finely spaced.

3 Model Parametrization and Simulations

We now show an example of how the DEM framework may be applied to CNTs. The DEM parametrization of a (5,5)@(10,10)@(15,15) multiwalled (MW) CNT is given in Tables 1–3. This MWCNT was parametrized as an elastic cylinder for use in the PFC3D simulations. This is a natural choice given the fact that the parallel bonds represent elastic cylinders. The

²Here, we used $\sigma = 3.851$ Å and $\epsilon = 4.0$ meV.

Table 1 DEM parametrization for a (5,5)@(10,10)@(15,15) MWCNT

m (amu)	R (Å)
2880	25.4

Table 2 Parallel bond parametrization for a (5,5)@(10,10)@(15,15) MWCNT

T (Å)	r (Å)	k_n (eV/Å ⁴)	k_s (eV/Å ⁴)
5.06	10.17	2.81	0.57

Table 3 Van der Waals bond parametrization for the interaction of (5,5)@(10,10)@(15,15) MWCNTs

ε' (meV)	A	B
10.77	9.15×10^{-4}	1.31

approximation does not introduce significant inaccuracies especially when the primary mode of deformation is bending as the space inside the (5,5) that is empty in the real CNT contributes less than 2% to its moment of inertia. The empty space contributes less than 12% to the cross-sectional area of the cylinder.

Parallel bond radius r is set to the radius of the outer (15,15) wall 10.17 Å. Each DEM sphere lumps two translational unit cells of the armchair MWCNT so the element spacing T is 5.06 Å. Each sphere then lumps 240 carbon atoms, giving each sphere a mass $m=2880$ amu, important if the dynamics are to be studied. The bending stiffness EI_x of this MWCNT, 12.0 eV μm , taken from a previous atomistic study [5] was used to calculate the Young modulus of the elastic cylinder representing the MWCNT $E=2.29$ TPa. The elastic modulus in shear was taken as the surface shear modulus of graphene multiplied by the interwall spacing of the MWCNT, 3.4 Å. The result is $G=459$ GPa. It was shown that only the innermost tubes' moduli are likely to slightly deviate from this value [3]. The error caused is further reduced by the fact that the fictitious area occupied by the inner walls contributes a comparatively small portion to the area and polar moment of the cylinder. Appropriately scaling by T , the discrete normal and shear stiffnesses for each parallel bond are then $k_n=2.81$ eV/Å⁴ and $k_s=0.57$ eV/Å⁴. Because the discrete elements must interpenetrate to interact, the radius of the discrete element, $R=25.4$ Å, is one-half the cutoff radius for the vdW interaction.

Having the model parametrized, we now demonstrate its utility in describing the MWCNT rings often encountered in experiment [22]. This represents an ideal test for the model since the ring structure arises from the energy balance stored in the parallel and vdW bonds. Simulations considered a (5,5)@(10,10)@(15,15) MWCNT of 500 nm length containing 240,000 atomic degrees of freedom, a system well beyond the comfortable computational level of atomistic or finite element simulations. This MWCNT is represented by 1000 DEM balls.

Starting from a straight configuration, the tube was gradually bent. During this process, strain accumulated in the parallel bonds while vdW bonds played a negligible role. The remarkable part starts from the moment when the two ends are brought into vdW contact. Focusing on this last part of the simulation, which lasted for about 2 h on a regular laptop computer, Fig. 2 shows the initial (top) and final obtained (bottom) configurations. Instead of returning to the initial straight state, the CNT evolves to the final stable ring shown on the bottom. This state, resulted by sliding of the two ends in the overlap region, as well as elastic relaxation, represents a minimum-energy state in the balance between vdW and elastic energy. Because the curvature of the ring is less than 0.2 nm^{-1} , placing it well within the linear elastic regime of bending [5], the parallel bond parametrization is valid.

4 Conclusion

On the surface, it could be difficult to see what a methodology designed for large-scale engineering problems has to do with CNT systems. In this paper, we indicated the suitability of this methodology on much smaller time and size scales. We represented each CNT with a chain of parallel-bonded spherical elements to capture the intrawall interactions along with a vdW model to capture interwall interactions. The resulting mesoscale model is adequate for implementation in existing DEM software packages. With the PFC3D code, we demonstrated its ability to describe CNT rings. Of course, the basic CNT mesoscopic model introduced here can be

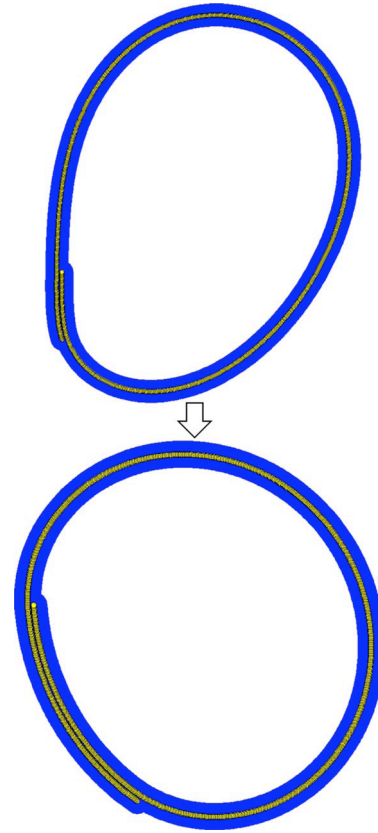


Fig. 2 Result of (5,5)@(10,10)@(15,15) MWCNT ring simulation showing initial and final configurations of relaxation. Light gray (yellow) represents the size of the CNT, while gray (blue) represents the vdW cutoff radii of each ball.

further optimized and enhanced. For example, the parallel bonds can be adjusted to accommodate nonlinear rippling by introducing a reduction in the relevant elastic constants beyond certain strain levels [5]. To describe CNT fracture, one can introduce bond strengths beyond which the parallel bonds break [1]. There is an interesting prospect for more complex engineering investigations since the foundations are already in place. For example, the method could be used to study bundling and coagulation of tubes in water supplies and blood streams, of high importance for the relatively recent area of nanotoxicology.

Acknowledgment

We thank NSF CAREER under Grant No. CMMI-0747684, NSF under Grant No. CMMI 0800896, and Itasca Education Partnership Program.

Nomenclature

- r = nanotube radius
- Y, G = Young and shear moduli of a carbon nanotube
- m, R = mass and radius of a distinct spherical element
- T, r = length and radius of the parallel bond
- k_n, k_s = normal and shear stiffnesses of a parallel bond
- ε', A, B = parameters for the van der Waals contact
- L = intertube center-to-center distance
- D = normalized intertube center-to-center distance
- $D=(L/r)-2$

Appendix

Equation (1) is an approximate evaluation of the vdW interaction energy given by the integral

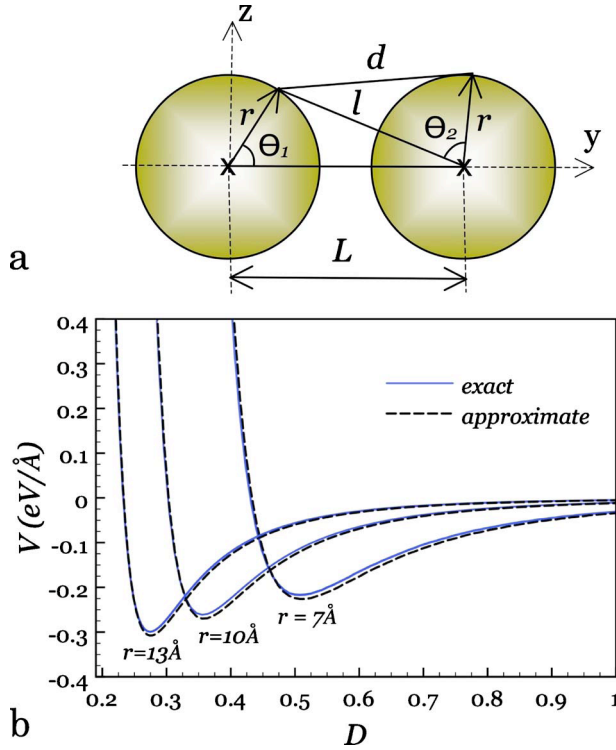


Fig. 3 (a) Schematics for the cross-sectional view of two parallel tubes. (b) The vdW energy versus a normalized intertube center-to-center distance D . Results are shown for three different tube radii. Both exact Eq. (A1) (numerical integration) and approximate Eq. (1) evaluations are presented for a comparison.

$$V(D) = \rho_c^2 r^2 T \int_{-\pi}^{\pi} \int_{-\pi}^{\pi} \int_{-T/2}^{T/2} v(d) dx d\theta_2 d\theta_1 \quad (A1)$$

In cylindrical coordinates (r, θ, x) , the distance between two atoms located on two different tube segments aligned along the x -axis is $d = \sqrt{r^2 + l^2 - 2rl \cos \theta_2 + x^2}$, where $l = \sqrt{r^2 + L^2 - 2rL \cos \theta_1}$ (Fig. 3(a)). We are focusing on the case in which the distance between tubes is small, which means $D \ll 1$. Then, the major contribution to Eq. (A1) comes from small angles θ_1 and θ_2 . It is convenient to introduce the notation $t = \sqrt{r^2 + l^2 - 2rl \cos \theta_2}$. Then, $t/r \ll 1$. If $T \sim r$, also, $t/T \ll 1$. Using these approximations in the attraction and repulsive terms of Eq. (A1), it follows that:

$$\int_{-T/2}^{T/2} \frac{dx}{d^6} = \int_{-T/2}^{T/2} \frac{dx}{(t^2 + x^2)^3} = \frac{3\pi}{8} \frac{1}{t^5} \left[1 + O\left(\frac{t}{T}\right) \right]$$

$$\int_{-T/2}^{T/2} \frac{dx}{d^{12}} = \int_{-T/2}^{T/2} \frac{dx}{(t^2 + x^2)^6} = \frac{63\pi}{256} \frac{1}{t^{11}} \left[1 + O\left(\frac{t}{T}\right) \right]$$

Neglecting the higher order terms, Eq. (A1) writes

$$V(D) \approx \varepsilon \rho_c^2 T \frac{3\pi\sigma^6}{2r^3} \int_{-\pi}^{\pi} \int_{-\pi}^{\pi} \left[\frac{21\sigma^6}{32r^6} \left(\frac{r}{t}\right)^{11} - \left(\frac{r}{t}\right)^5 \right] d\theta_2 d\theta_1 \quad (A2)$$

Further, using a Taylor series expansion

$$\frac{t^2}{r^2} = \theta_2^2 + (D + \theta_1^2)^2 + o(\max\{\theta_2^2, \theta_1^2, D\theta_1^2, D^2\}) \quad (A3)$$

and substituting Eq. (A3) into Eq. (A2), one recovers Eq. (1). The constants a and B are given by

$$a = \int_{-\infty}^{\infty} \int_{-\infty}^{\infty} \frac{dt_1 dt_2}{(t_2^2 + (1 + t_1^2)^{11/2})} \approx 0.47$$

$$B = \int_{-\infty}^{\infty} \int_{-\infty}^{\infty} \frac{dt_1 dt_2}{(t_2^2 + (1 + t_1^2)^{5/2})} \approx 1.31$$

The comparison for the vdW energy Eq. (A1) obtained by numerical integration against the approximate form given by Eq. (1) is presented in Fig. 3(b) for three values of r . The small-intertube approximation behind Eq. (1) works very well even for large D values. This is because the exact interaction energy at large distances is negligibly small.

References

- [1] Dumitrică, T., Hua, M., and Yakobson, B., 2006, "Symmetry-, Time-, and Temperature-Dependent Strength of Carbon Nanotubes," *Proc. Natl. Acad. Sci. U.S.A.*, **103**(16), pp. 6105–6109.
- [2] Yakobson, B., Brabec, C., and Bernholc, J., 1996, "Nanomechanics of Carbon Tubes: Instabilities Beyond Linear Response," *Phys. Rev. Lett.*, **76**(14), pp. 2511–2514.
- [3] Zhang, D.-B., and Dumitrică, T., 2008, "Elasticity of Ideal Single-Walled Carbon Nanotubes via Symmetry-Adapted Tight-Binding Objective Modeling," *Appl. Phys. Lett.*, **93**, p. 031919.
- [4] Zhang, D.-B., James, R., and Dumitrică, T., 2009, "Electromechanical Characterization of Carbon Nanotubes in Torsion via Symmetry Adapted Tight-Binding Objective Molecular Dynamics," *Phys. Rev. B*, **80**(11), p. 115418.
- [5] Nikiforov, I., Zhang, D.-B., James, R., and Dumitrică, T., 2010, "Wavelike Rippling in Multiwalled Carbon Nanotubes Under Pure Bending," *Appl. Phys. Lett.*, **96**, p. 123107.
- [6] Buehler, M., Kong, Y., and Gao, H., 2004, "Deformation Mechanisms of Very Long Single-Wall Carbon Nanotubes Subject to Compressive Loading," *ASME J. Eng. Mater. Technol.*, **126**(3), pp. 245–249.
- [7] Zhigilei, L., Wei, C., and Srivastava, D., 2005, "Mesoscopic Model for Dynamic Simulations of Carbon Nanotubes," *Phys. Rev. B*, **71**(16), p. 165417.
- [8] Duan, W. H., Wang, Q., Wang, Q., and Liew, K. M., 2010, "Modeling the Instability of Carbon Nanotubes: From Continuum Mechanics to Molecular Dynamics," *J. Nanotechnol. Eng. Med.*, **1**(1), p. 011001.
- [9] Arroyo, M., and Belytschko, T., 2003, "Nonlinear Mechanical Response and Rippling of Thick Multiwalled Carbon Nanotubes," *Phys. Rev. Lett.*, **91**(21), p. 215505.
- [10] Pantano, A., Boyce, M., and Parks, D., 2003, "Nonlinear Structural Mechanics Based Modeling of Carbon Nanotube Deformation," *Phys. Rev. Lett.*, **91**(14), p. 145504.
- [11] Tomblar, T. W., Zhou, C., Alexseyev, L., Kong, J., Dai, H., Liu, L., Jayanthi, C., Tang, M., and Wu, S.-Y., 2000, "Reversible Electromechanical Characteristics of Carbon Nanotubes Under Local-Probe Manipulation," *Nature (London)*, **405**, pp. 769–772.
- [12] 2001, *Polymer Nanocomposites: Processing, Characterization, and Applications*, R. Vaia and R. Krishnamoorti, eds., American Chemical Society, Washington, D.C.
- [13] Poland, C., Duffin, R., Kinloch, I., Maynard, A., Wallace, A. H., Seaton, A., Stone, V., Brown, S., MacNee, W., and Donaldson, K., 2008, "Carbon Nanotubes Introduced Into the Abdominal Cavity of Mice Show Asbestos-Like Pathogenicity in a Pilot Study," *Nat. Nanotechnol.*, **3**, pp. 423–428.
- [14] Hoogerbrugge, P., and Koelman, J., 1992, "Simulation Microscopic Hydrodynamic Phenomena With Dissipative Particle Dynamics," *Europhys. Lett.*, **19**(3), pp. 155–160.
- [15] Smith, D., and Harris, C., 1990, "Generalized Brownian Dynamics. I. Numerical Integration of the Generalized Langevin Equation Through Autoregressive Modeling of the Memory Function," *J. Chem. Phys.*, **92**(2), pp. 1304–1311.
- [16] Cundall, P., and Strack, O., 1979, "A Discrete Numerical Model for Granular Assemblies," *Geotechnique*, **29**(1), pp. 47–65.
- [17] Potyondy, D., and Cundall, P., 2004, "A Bonded-Particle Model for Rock," *Int. J. Rock Mech. Min. Sci.*, **41**(8), pp. 1329–1364.
- [18] Itasca Consulting Group Inc., 2008, *PF3D (Particle Flow Code in 3 Dimensions)*, Version 4.0. Minneapolis: ICG.
- [19] Plimpton, S., 1995, "Fast Parallel Algorithms for Short-Range Molecular Dynamics," *J. Comput. Phys.*, **117**(1), pp. 1–19.
- [20] 2010, *Trends in Computational Nanomechanics: Transcending Length and Time Scales*, T. Dumitrică, ed., Springer, New York.
- [21] Girifalco, L., Hodak, M., and Lee, R., 2000, "Carbon Nanotubes, Buckyballs, Ropes, and a Universal Graphitic Potential," *Phys. Rev. B*, **62**(19), pp. 13104–13110.
- [22] Martel, R., Shea, H. R., and Avouris, P., 1999, "Rings of Single-Walled Carbon Nanotubes," *Nature (London)*, **398**, p. 299.